ACS Photonics

Article

pubs.acs.org/journal/apchd5

Efficient Large-Area Transparent OLEDs Based on a Laminated Top Electrode with an Embedded Auxiliary Mesh

Sunghee Park,[†,‡,§] Jong Tae Lim,[†,§] Won-Yong Jin,[⊥,§] Hyunkoo Lee,[†] Byoung-Hwa Kwon,[†] Nam Sung Cho,[†] Jun-Han Han,[†] Jae-Wook Kang,[*,⊥] Seunghyup Yoo,[*,‡] and Jeong-Ik Lee[*,†]

[†]Flexible Information Device Research Section, Electronics and Telecommunications Research Institute, Daejeon 34129, Republic of Korea

[‡]School of Electrical Engineering, Korea Advanced Institute of Science and Technology (KAIST), Daejeon 34141, Republic of Korea

[⊥]Department of Flexible and Printable Electronics, Polymer Materials Fusion Research Center, Chonbuk National University, Jeonju 54896, Republic of Korea

S *Supporting Information*

ABSTRACT: To realize transparent organic light-emitting diodes (OLEDs), a top electrode should have excellent optical, electrical, and mechanical properties. Conventionally, transparent conductive oxides and semitransparent metal have been widely used for transparent top electrodes, but they have several fundamental drawbacks. We herein report efficient large-area inverted transparent OLEDs using a vacuum-laminated top electrode with an embedded metal mesh. The laminated device with 1 mm pitch exhibits superior optical properties including a high transmittance of 75.9% at 550 nm, a low reflectance of 12.0% at 550 nm, and spectrally flat characteristics over the entire visible region and shows nearly ideal Lambertian angular emission characteristics with little angular color shift in both directions. Moreover, the lowered sheet resistance of 4 Ω/sq originating from the embedded metal mesh (1 mm pitch) led to efficient and uniform emission characteristics. As a result, the device shows a relatively high maximum current efficiency of 50.3 cd/A (bottom: 24.5 cd/A; top: 25.8 cd/A) and a maximum external quantum efficiency of 15.3% (bottom: 7.9%; top: 7.4%), which surpasses all previously reported values based on a laminated top electrode. In addition, we successfully demonstrate its potential as a large-area transparent top electrode in various optoelectronic devices through a large-area transparent OLED segment panel (45 × 90 mm^2, diagonal length of 70.2 mm in the active area) with a laminated top electrode.

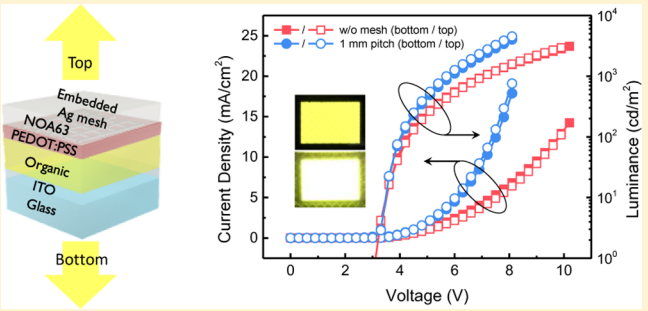

KEYWORDS: *organic light-emitting diodes (OLEDs), mesh embedded, transparent, top electrode, lamination*

Organic light-emitting diodes (OLEDs) have drawn attention for applications to high-end displays and have successfully been commercialized in the mobile display industry.[1−3] The focus of research is now being extended into large-area displays such as TVs as well as to those with unique form factors of flexibility and transparency.[4,5] In particular, transparent OLEDs (TOLEDs) are attractive because they can greatly extend the use of displays to emerging applications such as augmented reality, smart windows, head-up displays, and digital information displays.[6−8]

For TOLEDs, both the bottom and top electrodes should be transparent. In the case of the bottom electrode, various materials and processes can be utilized due to their low process limitation. On the other hand, many constraints exist for the top electrodes in TOLEDs. In general, the organic materials used in OLEDs are vulnerable to moisture, oxygen, plasma, and high temperature. Since the top electrodes are formed on the top organic layers constituting the OLEDs, the underlying organic layers should not be damaged during the energetic process such as either a plasma- or solution-based process. Choices are thus very limited. Semitransparent metals are typically used for the top electrode of TOLEDs due to the easy deposition process without damaging the organic layers. For instance, thin silver (Ag) has been recognized as an effective material for top electrodes; however, it has a low transmittance, high reflectance,[9,10] strong surface plasmon polariton (SPP) mode loss,[11−13] and relatively large angular color distortion in TOLEDs. Transparent conductive oxides (TCOs) such as indium−tin-oxide (ITO), indium−zinc-oxide (IZO), and aluminum−zinc-oxide (AZO) also may be considered as top electrodes in OLEDs owing to their superior optical and electrical properties, but they have a tendency to easily break under bending-induced strain, compared to other electrodes based on carbon, metal nanowires, and metal nanofibers, which recently have been developed and improved for use as

Received: November 25, 2016
Published: April 11, 2017

DOI: 10.1021/acsphotonics.6b00942
ACS Photonics 2017, 4, 1114−1122

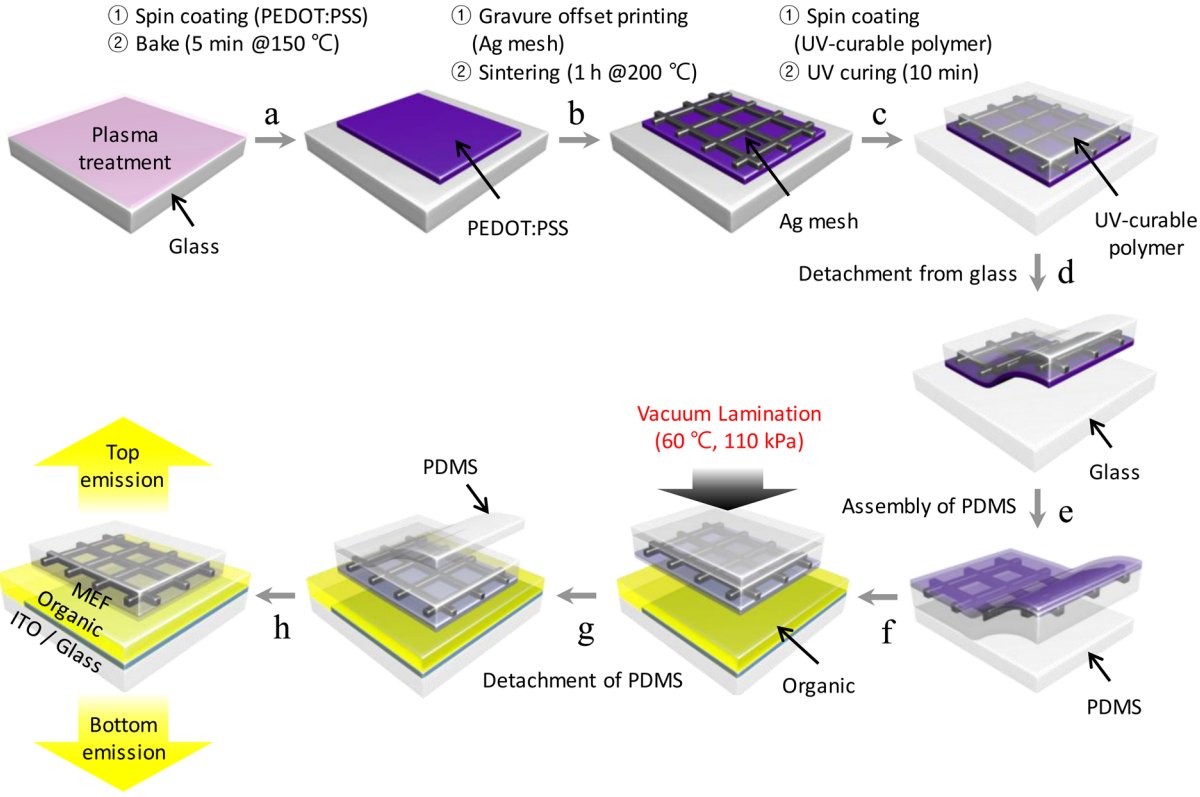

Figure 1. Overall fabrication process of transparent yellowish phosphorescent OLEDs with the proposed metal mesh embedded conductive film (MEF) using the vacuum lamination method.

transparent electrodes.[14−17] Moreover, the deposition of TCOs often causes physical damage such as both bombardment and charging damage to organic layers during the sputtering process.[18,19] Nonmetal materials such as graphene and conducting polymers have optically high transmittance and low reflectance in the visible spectral region, leading to minimal optical distortion. However, such nonmetal materials are difficult to deposit onto the organic layers in OLEDs without inducing damage because of the necessary harsh process conditions. Lim et al. previously reported TOLEDs with multilayered graphene (MLG) as nonmetal top electrodes by using a lamination method.[20] The device with the MLG top electrode showed good performance with negligible optical distortion. However, the MLG has high sheet resistance, and its electrical conductivity should be improved to allow its application to large-area displays.

To overcome the above challenges, we here propose a metal mesh embedded conductive film (MEF) as a new transparent top electrode in TOLEDs. The MEF consists of poly(3,4-ethylenedioxythiophene):poly(styrenesulfonate) (PEDOT:PSS) (Clevios PH1000, H.C.Starck), UV-curable polymer (NOA63, Norland Products Inc.), and an embedded Ag mesh. The TOLEDs are fabricated by a vacuum lamination process, leading to high charge injection from an air-free contact between the underlying organic layer and the MEF. The driving performance of the devices with the MEF, where the mesh pitches are 1, 2, and 4 mm, respectively, is shown to be superior to that of the device with only a PEDOT:PSS top electrode (hereinafter referred to as a metal mesh non-embedded conductive film (MNEF)). Furthermore, the MEF-laminated TOLEDs exhibit superior performance in terms of their optical properties, angular emission characteristics, and light-emitting efficiencies in comparison with those of conventional thin-Ag-based TOLEDs. A theoretical optical analysis is also carried out to investigate the factors underlying the improved performance and to verify the experimental results. A large transparent segment panel is then realized with the proposed laminated top electrode. These large-area devices exhibit significantly better performance than previous records based on a laminated top electrode,[21] demonstrating their potential for optoelectronic devices, as well as for large-area roll-to-roll and soluble OLEDs without any thermal-evaporation processes.

RESULTS AND DISCUSSION

Figure 1 schematically describes the overall fabrication process of the proposed inverted TOLEDs. We explain details with regard to the fabrication process conditions in the Methods section. For comparison, control devices were also fabricated with a thin Ag (20 nm) layer as a top electrode instead of the MEF. On the basis of many previous studies, the transmittance of the control devices could be improved by introducing a dielectric capping layer onto a thin Ag electrode.[22−25] Thus, for a more practical comparison, a capping layer of *N*,*N*′-diphenyl-*N*,*N*′-bis(1-naphthyl)-1,1′-biphenyl-4,4″-diamine (NPB) was additionally used on the control device.[26] The simulation results (Figure S1 of the Supporting Information (SI)) show that a total external quantum efficiency (η_{EQE}) of more than 20% can be achieved in the thin-Ag-based devices by designing a structure that utilizes the strong two-beam interference effect, and there have been other reports of similar results in various device structures.[25,27−29] However, in this case, the efficiency of the top emission is very low such that the luminance is quite different between the bottom and top emissions. In addition,

DOI: 10.1021/acsphotonics.6b00942
ACS Photonics 2017, 4, 1114−1122

the angular color distortion will be larger due to the strong two-beam interference effect. Therefore, the present thin-Ag-based control device structure with the capping layer thickness set at 60 nm was chosen so that the bottom and top emission efficiency can be maintained as close as possible.

Optical properties such as transmittance, haze, and reflectance of the MNEF (without the Ag mesh) and MEFs (1, 2, and 4 mm pitch) are measured in the whole visible spectral region (Figure 2a). The MNEF exhibited a total transmittance of 88.5% at 550 nm (including the substrate of NOA63). As the pitch of the embedded Ag mesh was increased, the total transmittance of the MEFs decreased from 86.5% (4 mm pitch) to 81.8% (1 mm pitch), which is even higher than that of the ITO glass substrate used in our study (Figure S2). The haze of the MEF (1 mm pitch) is only below 1.6% at 550 nm, which means that the embedded Ag mesh does not cause a haze effect because the mesh pitch is much larger than the visible wavelength. Also, the MEF (1 mm pitch) shows direct reflectance (measured by an aluminum reference) of only 7.2% and total reflectance (measured by a spectraloron reference) of 10.2% at 550 nm. In particular, the MEFs exhibited not only high transmittance and low reflectance but also spectrally flat characteristics in the whole visible range.

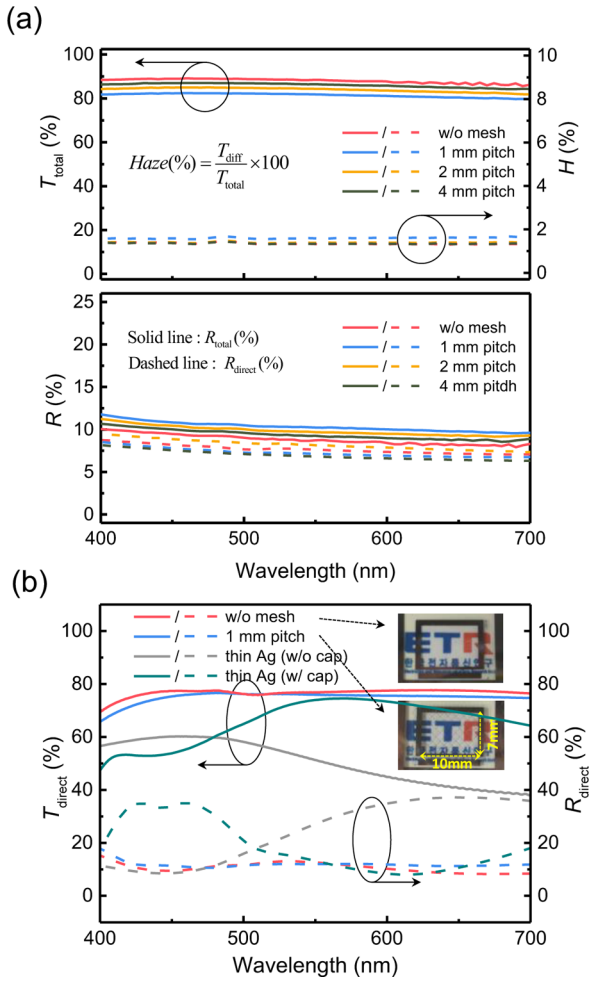

Figure 2. (a) Transmittance, haze, and reflectance of an MNEF (without mesh) and MEFs (1, 2, and 4 mm pitch). (b) Direct transmittance and reflectance of the devices with various top electrodes (insets in (b): the device images using the MNEF (without mesh) and the MEF (1 mm pitch) for top electrodes, respectively).

The direct transmittance and reflectance of the fabricated devices with the MNEF, MEF (1 mm pitch), and thin Ag (20 nm) top electrodes are shown in Figure 2b. The control device fabricated with thin Ag (w/o cap) exhibited a comparatively low transmittance of 51.3% and high reflectance of 27.1% at 550 nm.[20] Remarkably, as the wavelength increases above 500 nm, the transmittance of the thin-Ag-based device continuously drops below around 40% because of the increased reflectance. Meanwhile, the MNEF and MEF (1 mm pitch)-laminated devices exhibited notable characteristics, which kept up the spectrally flat optical properties, and showed high transmittances of 76.8% and 75.9% at 550 nm. At that time, their reflectances are 13.8% and 12.0%, respectively.

Figure 3a shows the angular distribution of the electroluminescence (EL) intensity between the MNEF-laminated device and the thin-Ag-based device, and the simulated results are also shown in Figure 3b and summarized in Table 1. The standard deviation of the angular intensity pattern from Lambertian angular emission (σ_{LB}) indicates how much the pattern deviates from the ideal Lambertian source and is defined by the following equation:[30]

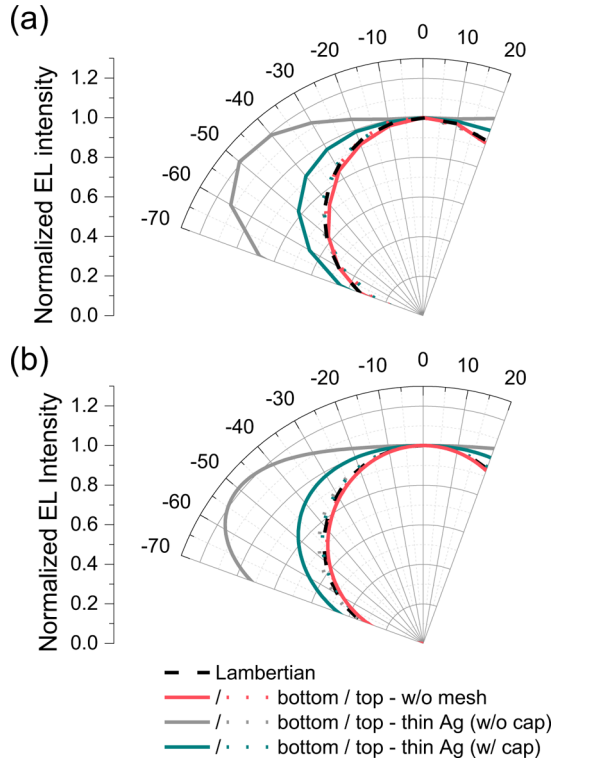

Figure 3. (a) Angular distribution of EL intensity between the MNEF (without mesh)-laminated device and the thin-Ag (without and with capping layer)-based devices and (b) simulated results.

$$\sigma_{LB} = \sqrt{\left(\sum_{i=1}^{N} [I(\theta_i)/I(0^\circ) - \cos\theta_i]^2\right)/N} \quad (1)$$

where θ_i denotes the observation angles, and we monitored at θ_i = 0−80° in this study. If the angular distribution of the EL intensity is close to the ideal Lambertian source, its values thus become closer to σ_{LB} = 0. The device based on the thin Ag (w/

DOI: 10.1021/acsphotonics.6b00942
ACS Photonics 2017, 4, 1114−1122

Table 1. Summary of Angular Emission Characteristics ($\Delta_{u'v'}$, $\bar{\Delta}_{u'v'}$, σ_{LB}) between the MNEF (without Mesh)-Laminated Device and the Thin-Ag-Based Devices (Values in Parentheses Are Simulated Results of σ_{LB})

	$\Delta_{u'v'}^{30°}$		$\Delta_{u'v'}^{60°}$		$\bar{\Delta}_{u'v'}$ (0–80°)		max $\Delta_{u'v'}$		σ_{LB}	
top electrode	bottom	top	bottom	top	bottom	top	bottom	top	bottom	top
MNEF (w/o mesh)	0.0017	0.0002	0.0056	0.0014	0.0030	0.0012	0.0059	0.0047	0.02 (0.02)	0.03 (0.02)
thin Ag (w/o cap)	0.0065	0.0012	0.0213	0.0033	0.0127	0.0017	0.0290	0.0033	0.40 (0.41)	0.02 (0.02)
thin Ag (w/cap)	0.0061	0.0021	0.0179	0.0071	0.0105	0.0037	0.0223	0.0083	0.11 (0.12)	0.03 (0.02)

o cap) top electrode shows an angular distribution that is quite far from the ideal Lambertian. This severe drawback originates from the two-beam interference effect introduced by a significant reflection from the metallic top electrodes.[31,32] The measured $\sigma_{LB.thin\ Ag\ (w/o\ cap)}$ values are 0.40 (bottom direction) and 0.02 (top direction), and the simulated values are 0.41 (bottom) and 0.02 (top) (Table 1). Despite that the capping layer was added to the thin-Ag-based device, the angular distribution was still distorted from ideal Lambertian. On the other hand, the MNEF-laminated device was measured to be nearly ideal Lambertian, and shown to have excellently well-balanced properties between the bottom and top directions due to the suppressed reflection of the top electrode. The measured $\sigma_{LB.MNEF}$ values were 0.02 (bottom) and 0.03 (top), and the simulated values were 0.02 (bottom) and 0.02 (top), respectively (Table 1).

To confirm the angular color changes, we measured the spectral variation depending on the observation angles. The color coordinates (x, y) in the International Commission on Illumination (CIE) 1931 of the thin-Ag (w/o cap)-based device at the bottom direction changed dramatically, as shown in Figure S3a. In particular, the normalized EL spectra at the front view (0 degree) showed significant differences between the bottom and top directions; indeed, a yellowish-green light (a peak wavelength of 553 nm) emitted in the top direction, while a yellowish light (a peak wavelength of 572 nm) was monitored in the bottom direction (Figure S3b). Additionally, the peak values in the bottom direction are seriously red-shifted as the viewing angle was increased (Figure S4a). Although the spectra variances are weakened in the capping-layer-added device, angular color changes are still observed in the bottom direction (Figure S4b). On the other hand, the MNEF-laminated devices present imperceptible differences of the angular color shift in both directions originating from the reduced reflectance of the top electrode (Figures S3 and S4).

For an intuitive grasp of the spectra variances, the color coordinates (x, y) in the CIE 1931 were converted into the u', v' color space in CIE 1976. The angular color shift at θ_i ($\Delta_{u'v'}^{\theta_i}$) and the mean angular color shift ($\bar{\Delta}_{u'v'}$) were calculated using the following equations:[30]

$$\Delta_{u'v'}^{\theta_i} = \sqrt{[\{u'(\theta_i) - u'(0°)\}^2 + \{v'(\theta_i) - v'(0°)\}^2]} \quad (2)$$

$$\bar{\Delta}_{u'v'} = \frac{1}{N}\sum_{i=1}^{N}\sqrt{[\{u'(\theta_i) - u'(0°)\}^2 + \{v'(\theta_i) - v'(0°)\}^2]} \quad (3)$$

In addition, the calculated angular color shift values are easily transformed into JNCD, where JNCD refers to just noticeable color difference and 1 JNCD = $\Delta_{u'v'}$ = 0.004.[33] In general, an angular color shift in the case of less than 3 JNCD is not visually noticeable on a display by the human eye. Consequently, the angular color shifts in various displays including OLEDs are desired to meet the required specification of $\Delta_{u'v'}$ < 3 JNCD. Calculated values of angular emission characteristics are summarized in Table 1 for the thin-Ag (w/o and w/cap)-based device and the MNEF-laminated device. The angular color shift at 30° ($\Delta_{u'v'}^{30°}$) of the thin-Ag-based device exhibited higher values compared to those of the MNEF-laminated device, and the value at 60° ($\Delta_{u'v'}^{60°}$) rapidly increased above 3 JNCD ($\Delta_{u'v'}$ = 0.012) in the bottom direction of the thin-Ag-based devices. Therefore, the mean angular color shift ($\bar{\Delta}_{u'v'}$) in the bottom direction of the thin-Ag-based devices showed around 3 JNCD. On the other hand, those of the MNEF-laminated device were maintained even below 1 JNCD for both directions. Especially, the maximum angular color shift of the MNEF-laminated device showed only around 1.5 JNCD ($\Delta_{u'v'}$ = 0.0059) and 1.2 JNCD ($\Delta_{u'v'}$ = 0.0047) (bottom and top), respectively, whereas a value of around 7.2 JNCD ($\Delta_{u'v'}$ = 0.0290), even more than twice the standard level of 3 JNCD, was observed in the bottom direction of the thin-Ag (w/o cap)-based device. Thus, the proposed laminated device is an excellent candidate for the display industry.

While the MNEF shows superior optical properties as mentioned above, it exhibits a sheet resistance of only around 250 Ω/sq.[34] So, it further needs to lower its sheet resistance to be large-area compatible.[35,36] By introducing the embedded Ag mesh (1 mm pitch), we achieved a sheet resistance of 4 Ω/sq.[34] In order to explore the potential for large-area display applications on the basis of the lowered sheet resistance of the MEFs, OLED devices were fabricated with a relatively large active area of 10 × 7 mm^2.

The current density–voltage–luminance (J–V–L) characteristics of the MNEF, the MEF-laminated, and the thin-Ag (w/o and w/cap)-based devices are shown in Figure 4a. The J–V curves were pulled forward as the Ag mesh pitches were decreased in the MEF-laminated devices. These results mean that the lowered sheet resistance resulting from the introduction of the Ag mesh enhanced the carrier conduction from the edge to the center of the active area of the top electrode without a significant voltage drop. Consequently, the MEF (1 mm pitch)-laminated device showed the most uniform and the brightest emitting properties at the same applied voltage of 5 V, as shown in the insets of Figure 4a. Notably, at the same applied voltage of 7.5 V, the MEF (1 mm pitch)-laminated device showed 2.5 times higher emissions (bottom: 2880 cd/m^2; top: 3263 cd/m^2) than those (bottom: 1219 cd/m^2; top: 1218 cd/m^2) of the MNEF-laminated device (Table 2). As expected, other devices with different Ag mesh pitches (2 and 4 mm pitch) exhibited higher luminance than those of the device based on the MNEF. In addition, the voltage–luminance (V–L) curves show relatively well-balanced luminance between the bottom and top directions because of the suppressed reflection of the top electrode, which makes the two-beam interference effect negligible (Figure 4a). However, the luminance between the bottom and top directions is quite different even in the case of the thin-Ag-based devices with the optimized capping layer (Figure 4a and Table 2). Figure 4b

DOI: 10.1021/acsphotonics.6b00942
ACS Photonics 2017, 4, 1114–1122

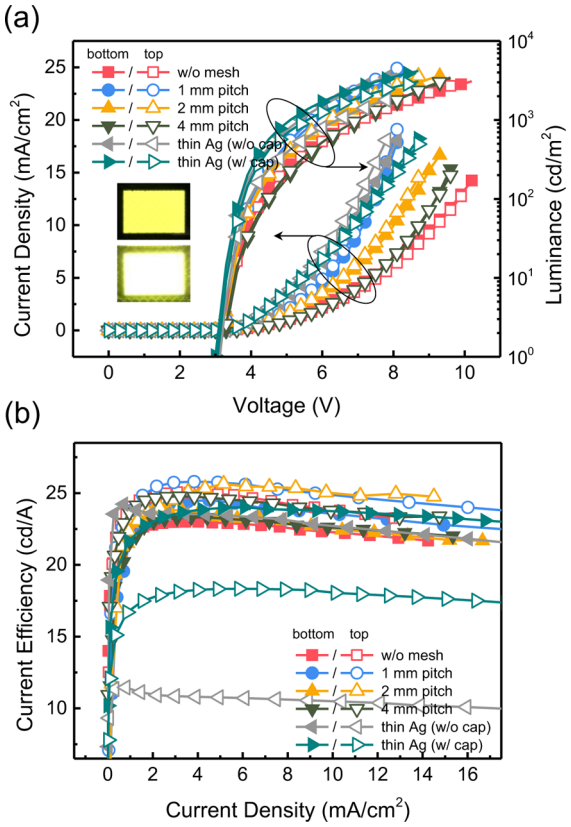

Figure 4. (a) Current density−voltage−luminance (J−V−L) and (b) current efficiency−current density (η_{CE}−J) characteristics of the MNEF, the MEF-laminated, and the thin-Ag (without and with capping layer)-based devices. (Insets in (a): emitting images of the MNEF (without mesh) and MEF (1 mm pitch)-laminated devices at 5 V.)

shows the current efficiency−current density (η_{CE}−J) characteristics of the MNEF and MEF-laminated devices and the thin-Ag (w/o and w/cap)-based devices. The maximum current efficiencies of the MEF-laminated devices exhibited similar values of around 24.5 ± 1.5 cd/A in both the bottom and top directions. Among them, the device with a 1 mm pitch shows the highest value of 50.3 cd/A (bottom: 24.5 cd/A; top: 25.8 cd/A) (Table 2). On the other hand, the current efficiencies in the top direction were considerably lower than those in the bottom direction in the thin-Ag-based devices.

The η_{EQE} value was evaluated in an integrating sphere system because the Ag mesh could block the light emission when measuring the angular light intensity. Indeed, the aperture ratio of MEF (1 mm pitch) was 92.2%, and thus the light emission could be blocked numerically by 7.8%. Despite the Ag mesh blocking some of the light emission, the maximum η_{EQE} of 15.3% (bottom: 7.9%; top: 7.4%) in the device based on MEF (1 mm pitch) was similar to the value of 15.4% (bottom: 7.5%; top: 7.9%) obtained in the MNEF-laminated device, which could not block the light emission, because of the lowered sheet resistance (Table 2).

For an optical analysis, contour plots of calculated power dissipation spectra as a function of the in-plane wavevector (k_x) for the device structure with the MNEF and thin Ag (w/o and w/cap) top electrode are presented in Figure 5a. Here, k_x denotes the projection of the total wave vector on the source plane. A highly significant amount of the power dissipation in surface plasmon polariton modes can be seen in the thin-Ag (w/o cap)-based device. The reduced SPP loss terms in the MNEF-laminated device can be clearly confirmed through the calculated power dissipation at 2.25 eV (λ = 550 nm), as shown in Figure 5b. This result is attributed to the constituents of the MNEF top electrode, which was fundamentally based on nonmetal materials. In order words, the MNEF has a much lower electron concentration than that of the thin Ag top electrode, and thus the weak SPP loss is generated at the interface of the MNEF/organic layer in the visible range. Even if the Ag mesh is embedded in the film, the SPP loss terms could be kept low because the Ag mesh is located at a fairly long distance from the emission dipoles, and the aperture ratio is very high (92.2% in the case of a 1 mm pitch). The calculated fractions of emitted optical power are provided in Table S1. The SPP loss modes are 4.0% and 16.2% for the MNEF-laminated device and thin-Ag (w/o cap)-based device, respectively. A sharp decline of the SPP loss was redistributed to the other modes. The calculated outcoupled mode of 15.5% (bottom: 7.5%; top: 8.0%) in the MNEF-laminated device is thus slightly improved compared to the value of 12.1% (bottom: 9.0%; top 3.1%) in the thin-Ag (w/o cap)-based device and is well consistent with the measured η_{EQE} value of 15.4% (bottom: 7.5%; top: 7.9%). Consequently, the absence of SPP loss in the laminated device is another advantage in terms of efficiency, and we can achieve more outcoupled efficiency using various light outcoupling techniques.

In addition, we demonstrated a large transparent segment panel (45 × 90 mm², diagonal length of 70.2 mm in the active area) with the laminated top electrode of the MEF (1 mm pitch) for further study of the suitability for large-area applications. The segment panel uniformly emitted in the whole active area as shown in Figure 6, and a movie clip is also available in Supporting Video 1. This successful demonstration

Table 2. Summary of Device Performance

device[a] (top electrode)		λ_{EL}(nm)[b]	CIE (x, y)[c]	V_{on} (V)[d]	L (cd/m²)[e]	CE_{max} (cd/A)[f]	EQE_{max} (%)[g]
MNEF	w/o mesh	552/553	(0.430, 0.555)/(0.429, 0.558)	3.1	1219/1218	23.0/25.1	7.5/7.9
MEF	1 mm pitch	551/553	(0.427, 0.557)/(0.426, 0.559)	3.1	2880/3263	24.5/25.8	7.9/7.4
	2 mm pitch	553/554	(0.430, 0.556)/(0.428, 0.558)	3.1	1799/2118	24.1/25.6	7.7/7.4
	4 mm pitch	553/553	(0.429, 0.557)/(0.428, 0.558)	3.1	1213/1325	23.3/24.8	7.5/7.5
thin Ag	w/o cap	572/553	(0.488, 0.504)/(0.434, 0.554)	3.1	3124/1607	24.2/11.5	8.9/3.3
	w/cap	561/555	(0.458, 0.533)/(0.434, 0.554)	3.1	3031/2232	24.0/18.3	8.3/6.0

[a]ITO (70 nm)/TRE:Li (5%, 30 nm)/TRE (25 nm)/Ir(ppy)$_2$(m-bppy):PGH02 (8%, 20 nm)/TcTa (10 nm)/TAPC (70 nm)/HAT-CN (30 nm)/various top electrodes. [b]Peak wavelength of EL spectra (bottom/top) at 7.5 V. [c]Color coordinates (CIE 1931) (bottom/top) at 7.5 V. [d]Applied voltage at a luminance of 1 cd/m². [e]Luminance (bottom/top) at 7.5 V. [f]Maximum current efficiency (bottom/top). [g]Maximum external quantum efficiency measured in integrating sphere system.

DOI: 10.1021/acsphotonics.6b00942
ACS Photonics 2017, 4, 1114−1122

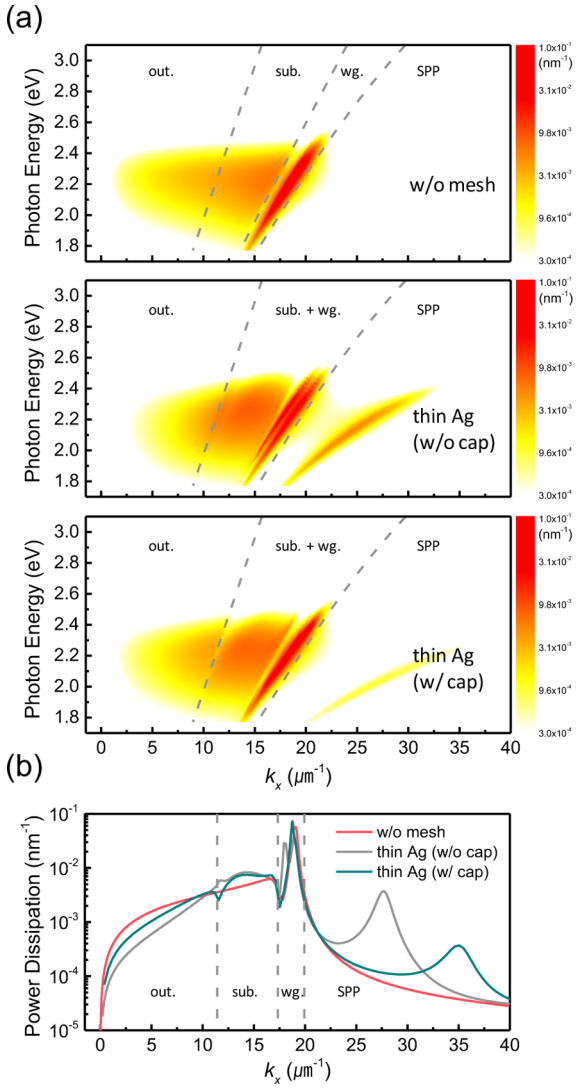

Figure 5. (a) Calculated power dissipation spectra weighted with the normalized emitter spectrum for the device structures with the MNEF (without mesh) and the thin Ag (without and with capping layer) top electrodes, respectively, and (b) calculated power dissipation at the photon energy of 2.25 eV (λ = 550 nm). The dashed lines denote the interface dividing the regions corresponding to outcoupled (out.), substrate-confined (sub.), waveguided (wg.), and surface plasmon polariton (SPP) modes, respectively.

substantiates the suitability of the MEF technology for various optoelectronic devices and large-area applications.

CONCLUSION

In summary, we fabricated efficient large-area inverted TOLEDs with the MEF top electrode using the vacuum lamination method. The lamination process was mild enough not to cause damage to the underlying organic layers. The MEF (1 mm pitch)-laminated devices exhibited not only superior optical properties such as a high transmittance of 75.9% at 550 nm, low reflectance of 12.0% at 550 nm, and spectrally flat characteristics in the whole visible ranges but also nearly ideal Lambertian angular emission characteristics with an almost negligible angular color shift in both the bottom and top directions. Furthermore, the lowered sheet resistance led to efficient and uniform emission properties over a large area. As a result, the MEF (1 mm pitch)-laminated device beats all

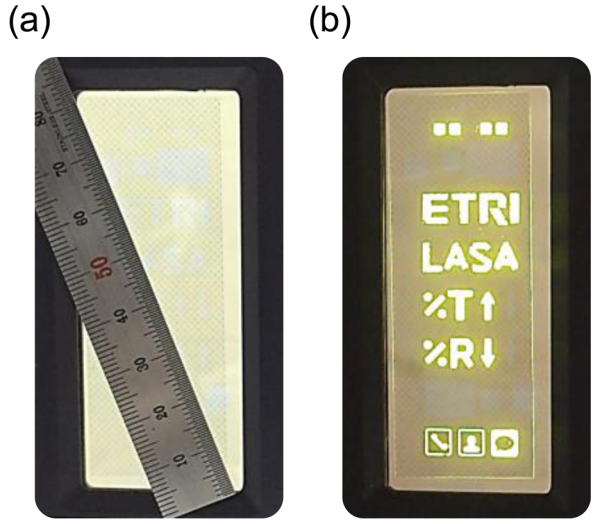

Figure 6. (a) Off-state image of the 45 × 90 mm^2 transparent segment panel (diagonal length of 70.2 mm in active area) with the laminated top electrode of the MEF (1 mm pitch) and (b) working image at 5 V.

previous records based on a laminated top electrode,[21] showing a relatively high maximum current efficiency of 50.3 cd/A (bottom: 24.5 cd/A; top: 25.8 cd/A) and a maximum external quantum efficiency of 15.3% (bottom: 7.9%; top: 7.4%). In addition, we successfully demonstrated a large transparent segment panel with the laminated top electrode of the MEF (1 mm pitch) to verify its suitability for large-area applications. We believe that the MEF technology is likely to make a great contribution to diverse flexible and transparent optoelectronic devices, as well as large-area roll-to-roll and soluble OLEDs without any thermal-evaporation processes.

METHODS

Top Electrode (MEF) Preparation and Characterization. First, a glass substrate was pretreated with a nitrogen (N_2) plasma (GENIA Tech) for making a hydrophilic surface. The PEDOT:PSS top electrode was spin-coated at 2000 rpm for 60 s onto the plasma-treated glass substrate followed by annealing at 150 °C for 5 min. In addition, the surface was treated with ethylene glycol (Aldrich, 99.8%) to improve the conductivity and wetting property[37] and was annealed at 150 °C for 5 min in ambient air. The Ag mesh was subsequently embedded between the PEDOT:PSS and NOA63 layers using the gravure offset printing method (DCN Co, Ltd., roll printer).[38] The Ag meshes were printed with various pitches between the Ag meshes. The fabricated MNEF, namely, a ~90-nm-thick PEDOT:PSS top electrode, exhibited a sheet resistance (R_{sheet}) value of ~250 Ω/sq, while the R_{sheet} values of the MEF with mesh pitches of 1, 2, and 4 mm were ~4, ~9, and ~19 Ω/sq, respectively.[34] A noncontact resistance measurement instrument (Napso, EC-80 P) was then used for accurate measurement of the R_{sheet}. In the MEF, the Ag mesh with a thickness of ~32 μm and a width of ~1.5 μm-embedded PEDOT:PSS layer served as a transparent conducting electrode, and a ~50-μm-thick NOA63 layer was employed as a supporting film.[34] The root-mean-square surface roughness (R_q) of the MEF was measured to be only less than 1 nm and the maximum peak-to-valley height (R_{pv}) was less than 7 nm.[34] These extremely smooth surfaces play an important role in the stable lamination process and efficient and uniform charge injection at the interface between the top organic layer

DOI: 10.1021/acsphotonics.6b00942
ACS Photonics 2017, 4, 1114−1122

and the surface of the MEF. The thickness and width were measured by surface profilometry (KLA Tencor, P-10), and R_q and R_{pv} were obtained using atomic force microscopy (AFM, Park Systems, NX-10), respectively. Figure S5 shows the spectrum obtained from ultraviolet photoemission spectroscopy (UPS, Pohang Accelerator Laboratory) measurements of the MEF (1 mm pitch).[39] The work function of ∼5.09 eV is estimated by subtracting the cutoff value from the excitation source (He I) of 21.2 eV. This high work function is sufficient for the proposed MEF to serve as an anode in OLEDs.[37,40]

TOLED Fabrication and Measurements. There are three important steps to fabricate the TOLEDs: (i) production of MEF (PEDOT:PSS/embedded Ag mesh/NOA63 film) on top of a plasma-treated glass substrate (Figure 1a−d); (ii) assembly of polydimethylsiloxane (PDMS, SYLGARD 184, Dow Corning Co.) with MEF (Figure 1e); and (iii) fabrication of TOLEDs by laminating the MEF onto the OLED stack consisting of glass/ITO/organic layers (Figure 1f−h). The vacuum lamination process (Figure 1f) was carried out through two main steps in an N_2-filled glovebox. The first step is to remove the air between the OLED stack and the MEF for 5 min in a vacuum environment, and thereafter the second step is to bond the interface of the PEDOT:PSS layer in the MEF and the adjacent organic layer by applying a pressure of approximately 110 kPa onto the PDMS for 5 min. Also, to avoid thermal damage to the underlying organic layers, the vacuum lamination was performed at a low temperature of 60 °C. Among the organic materials constituting the OLED stack, 1,1-bis((di-4-tolylamino)phenyl)cyclohexane (TAPC) has the lowest glass transition temperature (T_g) of 78 °C.[41] During the lamination process, the PDMS homogenizes the applied force on the underlying structures. As a result of this stable process, the luminance decay of the MNEF-laminated device was similar to that of the thin-Ag (w/cap)-based device at a constant driving current of 1 mA and room temperature, as shown in Figure S6.

In this study, the proposed inverted TOLEDs were made with the following configuration: glass as a substrate/ITO (70 nm) as a cathode/TRE:lithium (Li) (5%, 30 nm) as an electron injection layer (EIL)/TRE (25 nm) as an electron transport layer (ETL) and a hole blocking layer (HBL)/bis(2-phenylpyridinato)[2-(biphenyl-3-yl)pyridinato]iridium(III) (Ir(ppy)$_2$(m-bppy)):PGH02 (Duksan Hi-Metal Co., Ltd.)[42] (8%, 20 nm) as a yellowish emitting layer (EML)/4,4′,4″-tris(*N*-carbazolyl)-triphenylamine (TcTa) (10 nm) as an electron blocking layer (EBL)/TAPC (70 nm) as a hole transport layer (HTL)/1,4,5,8,9,11-hexaazatriphenylene-hexacarbonitrile (HAT-CN) as a hole injection layer (HIL) (30 nm)/metal mesh embedded conductive film as an anode. (TRE and PGH02 are proprietary materials.)

All organic and thin Ag layers were sequentially vacuum-deposited in a cluster chamber without breaking the vacuum at less than 5×10^{-7} Torr. After the lamination process, the MEF-laminated OLEDs were moved to an N_2-filled glovebox to be encapsulated with a glass lid containing a moisture getter and an edge sealant of ultraviolet (UV)-curable epoxy.

Transmittance, reflectance, and haze of the devices were measured through an ultraviolet−visible−near-infrared (UV−vis−NIR) spectrophotometer (Lambda 750 and 950, PerkinElmer). The current density−voltage (J−V) characteristics of the devices were measured using a Keithley-238 source-measurement unit, and the luminance and electroluminescence spectra were measured using a spectro-radiometer (CS-2000, Konica Minolta). External quantum efficiencies (η_{EQE}) were observed in an integrating sphere system (HM series, Otsuka Electronics). All measurements were carried out at room temperature.

Theoretical Simulation. The power dissipation spectra simulation was conducted on the basis of an advanced classical dipole model, which takes into account the Purcell effect, dipole orientation effect, and so on.[43−47] In this simulation, the refractive indexes of the used materials were measured by spectroscopic ellipsometry except for NOA63, which was referenced from the specification data on the Web site of Norland Products Inc. The anisotropic dipole orientation factor of emitting molecules (Ir(ppy)$_2$(m-bppy):PGH02) was assumed to be 1/3; that is, they are isotropically oriented dipoles. In addition, we assumed that the intrinsic emitter photoluminescence quantum yield and the hole−electron charge balancing were unity and the emission zone was placed at the ETL/EML interface.

■ ASSOCIATED CONTENT

Supporting Information

The Supporting Information is available free of charge on the ACS Publications website at DOI: 10.1021/acsphotonics.6b00942.

Additional information on the calculated fraction of emitted optical power in devices, the simulated maximum external quantum efficiency results, the transmittance of the various top electrodes and ITO substrate, variances of the color coordinates and EL spectra, the angular EL spectra, the UPS spectrum of the MEF, the luminance decay curves, and the demonstration of the 45 × 90 mm^2 transparent segment panel (PDF)

■ AUTHOR INFORMATION

Corresponding Authors

*E-mail: jwkang@jbnu.ac.kr.
*E-mail: syoo_ee@kaist.ac.kr.
*E-mail: jiklee@etri.re.kr.

ORCID

Sunghee Park: 0000-0001-5796-4933

Author Contributions

§S. Park, J. T. Lim, and W.-Y. Jin contributed equally to this work.

Notes

The authors declare no competing financial interest.

■ ACKNOWLEDGMENTS

This work was partly supported by an Institute for Information & Communications Technology Promotion (IITP) grant funded by the Korea government (MSIP) (B0101-16-0133, the core technology development of light and space adaptable energy-saving I/O platform for future advertising service), the Nano·Material Technology Development Program through the National Research Foundation of Korea (NRF) funded by the Ministry of Science, ICT and Future Planning (NRF-2016M3A7B4910631), and the Pioneer Research Center Program through the National Research Foundation of Korea (NRF) funded by the Ministry of Science, ICT and Future Planning (NRF-2013M3C1A3065528).

DOI: 10.1021/acsphotonics.6b00942
ACS Photonics 2017, 4, 1114−1122

REFERENCES

(1) Tang, C. W.; VanSlyke, S. A. Organic Electroluminescent Diodes. *Appl. Phys. Lett.* **1987**, *51*, 913−915.
(2) Tang, C. W.; VanSlyke, S. A.; Chen, C. H. Electroluminescence of Doped Organic Thin Films. *J. Appl. Phys.* **1989**, *65*, 3610−3616.
(3) Kim, S. W.; Hwang, B. H.; Lee, J. H.; Kang, J. I.; Min, K. W.; Kim, W. Y. 2.4-in. Monochrome Small Molecular OLED Display for Mobile Application. *Curr. Appl. Phys.* **2002**, *2*, 335−338.
(4) Shin, H.-J.; Takasugi, S.; Park, K.-M.; Choi, S.-H.; Jeong, y.-S.; Song, B.-C.; Kim, H.-S.; Oh, C.-H.; Ahn, B.-C. Novel OLED Display Technologies for Large-Size UHD OLED TVs. *Dig. Tech. Pap. - Soc. Inf. Disp. Int. Symp.* **2015**, *46*, 53−56.
(5) Jin, D.-U.; Lee, J.-S.; Kim, T.-W.; An, S.-G.; Straykhilev, D.; Pyo, Y.-S.; Kim, H.-S.; Lee, D.-B.; Mo, Y.-G.; Kim, H.-D.; Chung, H.-K. World-Largest (6.5″) Flexible Full Color Top Emission AMOLED Display on Plastic Film and Its Bending Properties. *Dig. Tech. Pap. - Soc. Inf. Disp. Int. Symp.* **2009**, *40*, 983−985.
(6) Gu, G.; Bulović, V.; Burrows, P. E.; Forrest, S. R. Transparent Organic Light Emitting Devices. *Appl. Phys. Lett.* **1996**, *68*, 2606−2608.
(7) Parthasarathy, G.; Burrows, P. E.; Khalfin, V.; Kozlov, V. G.; Forrest, S. R. A Metal-Free Cathode for Organic Semiconductor Devices. *Appl. Phys. Lett.* **1998**, *72*, 2138−2140.
(8) Yang, U.; Kim, N.-G; Kim, K.-H. Augmented System for Immersive 3D Expansion and Interaction. *ETRI Journal* **2016**, *38*, 149−158.
(9) Hung, L.-S.; Madathil, J. Reduction of Ambient Light Reflection in Organic Light-Emitting Diodes. *Adv. Mater.* **2001**, *13*, 1787−1790.
(10) Sung, W. J.; Lee, J.; Joo, C. W.; Cho, N. S.; Lee, H.; Lee, G.-W.; Lee, J.-I. Colored Semi-Transparent Organic Light-Emitting Diodes. *J. Inf. Disp.* **2014**, *15*, 177−184.
(11) Wedge, S.; Wasey, J. A. E.; Barnes, W. L.; Sage, I. Coupled Surface Plasmon-Polariton Mediated Photoluminescence from a Top-Emitting Organic Light-Emitting Structure. *Appl. Phys. Lett.* **2004**, *85*, 182−184.
(12) Wedge, S.; Hooper, I. R.; Sage, I.; Barnes, W. L. Light Emission Through a Corrugated Metal Film: The Role of Cross-Coupled Surface Plasmon Polaritons. *Phys. Rev. B: Condens. Matter Mater. Phys.* **2004**, *69*, 245418.
(13) Hobson, P. A.; Wedge, S.; Wasey, J. A. E.; Sage, I.; Barnes, W. L. Surface Plasmon Mediated Emission from Organic Light-Emitting Diodes. *Adv. Mater.* **2002**, *14*, 1393−1396.
(14) Langley, D.; Giusti, G.; Mayousse, C.; Celle, C.; Bellet, D.; Simonato, J.-P. Flexible Transparent Conductive Materials Based on Silver Nanowire Networks: A Review. *Nanotechnology* **2013**, *24*, 452001.
(15) Hecht, D. S.; Hu, L.; Irvin, G. Emerging Transparent Electrodes Based on Thin Films of Carbon Nanotubes, Graphene, and Metallic Nanostructures. *Adv. Mater.* **2011**, *23*, 1482−1513.
(16) Lee, Y.; Min, S.-Y.; Kim, T.-S.; Jeong, S.-H.; Won, J. Y.; Kim, H.; Xu, W.; Jeong, J. K.; Lee, T.-W. Versatile Metal Nanowiring Platform for Large-Scale Nano and Opto-Electronic Devices. *Adv. Mater.* **2016**, *28*, 9109−9116.
(17) Lee, Y.; Kim, T.-S.; Min, S.-Y.; Xu, W.; Jeong, S.-H.; Seo, H.-K.; Lee, T.-W. Individually Position-Addressable Metal-Nanofiber Electrodes for Large-Area Electronics. *Adv. Mater.* **2014**, *26*, 8010−8016.
(18) Lee, J.-H.; Lee, S.; Kim, J.-B.; Jang, J.; Kim, J.-J. A High Performance Transparent Inverted Organic Light Emitting Diode with 1,4,5,8,9,11-Hexaazatriphenylenehexacarbonitrile as an Organic Buffer Layer. *J. Mater. Chem.* **2012**, *22*, 15252−15266.
(19) Dobbertin, T.; Kroeger, M.; Heithecker, D.; Schneider, D.; Metzdorf, D.; Neuner, H.; Becker, E.; Johannes, H.-H.; Kowalsky, W. Inverted Top-Emitting Organic Light-Emitting Diodes using Sputter-Deposited Anodes. *Appl. Phys. Lett.* **2003**, *82*, 284−286.
(20) Lim, J. T.; Lee, H.; Cho, H.; Kwon, B.-H.; Cho, N. S.; Lee, B. K.; Park, J.; Kim, J.; Han, J.-H.; Yang, J.-H; Yu, B.-G.; Hwang, C.-S.; Lim, S. C.; Lee, J.-I. Flexion Bonding Transfer of Multilayered Graphene as a Top Electrode in Transparent Organic Light-Emitting Diodes. *Sci. Rep.* **2015**, *5*, 17748.
(21) Lin, C.-Y.; Hu, N.-W.; Chang, H.-W.; Lu, C.-Y.; Chen, C.-Y.; Wu, C.-C. Efficient Transparent Small-Molecule Organic Light-Emitting Devices Adopting Laminated Transparent Top Electrodes. *Org. Electron.* **2016**, *28*, 25−30.
(22) Riel, H.; Karg, S.; Beierlein, T.; Rieß, W.; Neyts, K. Tuning the Emission Characteristics of Top-Emitting Organic Light-Emitting Devices by Means of a Dielectric Capping Layer: An Experimental and Theoretical Study. *J. Appl. Phys.* **2003**, *94*, 5290−5296.
(23) Hung, L. S.; Tang, C. W.; Mason, M. G.; Raychaudhuri, P.; Madathil, J. Application of an Ultrathin LiF/Al Bilayer in Organic Surface-Emitting Diodes. *Appl. Phys. Lett.* **2001**, *78*, 544−546.
(24) Huang, Q.; Walzer, K.; Pfeiffer, M.; Leo, K.; Hofmann, m.; Stübinger, T. Performance Improvement of Top-Emitting Organic Light-Emitting Diodes by an Organic Capping Layer: An Experimental Study. *J. Appl. Phys.* **2006**, *100*, 064507.
(25) Chung, J.; Cho, H.; Koh, T.-W.; Lee, J.; Kim, E.; Lee, J.; Lee, J.-I.; Yoo, S. Towards Highly Efficient and Highly Transparent OLEDs: Advanced Considerations for Emission Zone Coupled with Capping Layer Design. *Opt. Express* **2015**, *23*, 247472.
(26) Huh, J. W.; Moon, J.; Lee, J. W.; Cho, D.-H.; Shin, J.-W.; Han, J.-H.; Hwang, J.; Joo, C. W.; Lee, J.-I.; Chu, H. Y. The Optical Effects of Capping Layers on the Performance of Transparent Organic Light-Emitting Diodes. *IEEE Photonics J.* **2012**, *4*, 39−47.
(27) Lee, J.; Hofmann, S.; Furno, M.; Thomschke, M.; Kim, Y. H.; Lüssem, B.; Leo, K. Influence of Organic Capping Layers on the Performance of Transparent Organic Light-Emitting Diodes. *Opt. Lett.* **2011**, *36*, 1443−1445.
(28) Kim, Y. H.; Lee, J.; Hofmann, S.; Gather, M. C.; Müller-Meskamp, L.; Leo, K. Achieving High Efficiency and Improved Stability in ITO-Free Transparent Organic Light-Emitting Diodes with Conductive Polymer Electrodes. *Adv. Funct. Mater.* **2013**, *23*, 3763−3769.
(29) Schwab, T.; Schubert, S.; Hofmann, S.; Fröbel, M.; Fuchs, C.; Thomschke, M.; Müller-Meskamp, L.; Leo, K.; Gather, M. C. Highly Efficient Color Stable Inverted White Top-Emitting OLEDs with Ultra-Thin Wetting Layer Top Electrodes. *Adv. Opt. Mater.* **2013**, *1*, 707−713.
(30) Lee, J.; Han, T.-H.; Park, M.-H.; Jung, D. Y.; Seo, J.; Seo, H.-K; Cho, H.; Kim, E.; Chung, J.; Choi, S.-Y.; Kim, T.-S.; Lee, T.-W.; Yoo, S. Synergetic Electrode Architecture for Efficient Graphene-Based Flexible Organic Light-Emitting Diodes. *Nat. Commun.* **2016**, *7*, 11791.
(31) Schubert, E. F.; Hunt, N. E. J.; Micovic, M.; Malik, R. J.; Sivco, D. L.; Cho, A. Y.; Zydzik, G. J. Highly Efficient Light-Emitting Diodes with Microcavities. *Science* **1994**, *265*, 943−945.
(32) Neyts, K. Microcavity Effects and the Outcoupling of Light in Displays and Lighting Applications Based on Thin Emitting Films. *Appl. Surf. Sci.* **2005**, *244*, 517−523.
(33) Steckel, J. S.; Ho, J.; Hamilton, C.; Xi, J.; Breen, C.; Liu, W.; Allen, P.; Coe-Sullivan, S. Quantum Dots: The Ultimate Down-Conversion Material for LCD Displays. *J. Soc. Inf. Disp.* **2015**, *23*, 294−305.
(34) Jin, W.-Y.; Ginting, R. T.; Ko, K.-J.; Kang, J.-W. Ultra-Smooth, Fully Printed Large-Area Transparent Conducting Electrodes for Organic Devices. *Sci. Rep.* **2016**, *6*, 36475.
(35) Neyts, K.; Marescaux, M.; Nieto, A. U.; Elschner, A.; Lövenich, W.; Fehse, K.; Huang, Q.; Walzer, K.; Leo, K. Inhomogeneous Luminance in Organic Light Emitting Diodes Related to Electrode Resistivity. *J. Appl. Phys.* **2006**, *100*, 114513.
(36) Slawinski, M.; Weingarten, M.; Heuken, M.; Vescan, A.; Kalisch, H. Investigation of Large-Area OLED Devices with Various Grid Geometries. *Org. Electron.* **2013**, *14*, 2387−2391.
(37) Li, Z.; Qin, F.; Liu, T.; Ge, R.; Meng, W.; Tong, J.; Xiong, S.; Zhou, Y. Optical Properties and Conductivity of PEDOT:PSS Films Treated by Polyethylenimine Solution for Organic Solar Cells. *Org. Electron.* **2015**, *21*, 144−148.
(38) Jung, S.; Lee, S.; Song, M.; Kim, D.-G.; You, D. S.; Kim, J.-K.; Kim, C. S.; Kim, T.-M.; Kim, K.-H; Kim, J.-J.; Kang, J.-W. Extremely

DOI: 10.1021/acsphotonics.6b00942
ACS Photonics 2017, 4, 1114−1122

Flexible Transparent Conducting Electrodes for Organic Devices. *Adv. Energy Mater.* **2014**, *4*, 1300474.
(39) Jiang, X.; Wong, F. L.; Fung, M. K.; Lee, S. T. Aluminum-Doped Zinc Oxide Films as Transparent Conductive Electrode for Organic Light-Emitting Devices. *Appl. Phys. Lett.* **2003**, *83*, 1875−1877.
(40) Zhou, Y.; Fuentes-Hernandez, C.; Shim, J.; Meyer, J.; Giordano, A. J.; Li, H.; Winget, P.; Papadopoulos, T.; Cheun, H.; Kim, J.; Fenoll, M.; Dindar, A.; Haske, W.; Najafabadi, E.; Khan, T. M.; Sojoudi, H.; Barlow, S.; Graham, S.; Brédas, J.-L.; Marder, S. R.; Kahn, A.; Kipplelen, B. A Universal Method to Produce Low-Work Function Electrodes for Organic Electronics. *Science* **2012**, *336*, 327−332.
(41) Yeh, H.-C.; Meng, H.-F.; Lin, H.-W.; Chao, T.-C.; Tseng, M.-R.; Zan, H.-W. All-Small-Molecule Efficient White Organic Light-Emitting Diodes by Multi-Layer Blade Coating. *Org. Electron.* **2012**, *13*, 914−918.
(42) Park, J. W.; Kim, T. W.; Park, J. B. Investigation on a Short Circuit of Large-Area OLED Lighting Panels. *Semicond. Sci. Technol.* **2013**, *28*, 045013.
(43) Purcell, E. M.; Torrey, H. C.; Pound, R. V. Resonance Absorption by Nuclear Magnetic Moments in a Solid. *Phys. Rev.* **1946**, *69*, 37.
(44) Neyts, K. Simulation of Light Emission from Thin-Film Microcavities. *J. Opt. Soc. Am. A* **1998**, *15*, 962−971.
(45) Barnes, W. L. Fluorescence Near Interfaces: The Role of Photonic Mode Density. *J. Mod. Opt.* **1998**, *45*, 661−699.
(46) Furno, M.; Meerheim, R.; Hofmann, S.; Lüssem, B.; Leo, K. Efficiency and Rate of Spontaneous Emission in Organic Electroluminescent Devices. *Phys. Rev. B: Condens. Matter Mater. Phys.* **2012**, *85*, 115205.
(47) Fuchs, C.; Will, P.-A.; Wieczorek, M.; Gather, M. C.; Hofmann, S.; Reineke, S.; Leo, K.; Scholz, R. Enhanced Light Emission from Top-Emitting Organic Light-Emitting Diodes by Optimizing Surface Plasmon Polariton Losses. *Phys. Rev. B: Condens. Matter Mater. Phys.* **2015**, *92*, 245306.

DOI: 10.1021/acsphotonics.6b00942
ACS Photonics 2017, 4, 1114−1122